IET Electric Power Applications

*Research Article*

IET Journals
The Institution of Engineering and Technology

# Analysis and design of diverse electromagnet type actuators for moulded case circuit breaker

ISSN 1751-8660
Received on 17th January 2016
Revised on 25th May 2016
Accepted on 10th June 2016
doi: 10.1049/iet-epa.2016.0015
www.ietdl.org

*Hyeon-Jeong Park[1], Hyun-Kyo Jung[1], Jong-Suk Ro[2]* ✉

[1]*Department of Electrical and Computer Engineering, Seoul National University, San 56-1, Shinlim-Dong, Kwanak-Gu, Seoul 151-742, Korea*
[2]*School of Electrical and Electronics Engineering, Chung-Ang University, Dongjak-gu, Seoul, Korea*
✉ *E-mail: jongsukro@naver.com*

**Abstract:** Recently, remote-controllable actuators for circuit breaker (CB) have attracted attention for the smart grid electric power system. In this study, diverse kinds of remote-controllable electromagnetic actuator for CB are precisely investigated to give a guideline for the selection of the effective actuator according to numerous voltage level of CB. In case of a low-voltage level of CB, the separated permanent-magnet actuator (SPMA) is verified in this research as the most suitable actuator through the comparison with diverse electromagnetic actuators. The SPMA is designed for the 225AF moulded case CB by using the proposed optimisation method, which the authors termed as a multi-step optimisation strategy.

## 1 Introduction

Circuit breakers (CBs) protect distribution systems from a faulty current caused by overloads, short circuits, or other abnormal circumstances. When the CB abruptly opens current-carrying circuits, a strong arc is generated across contacts. Therefore, the CB should ensure that the contacts are separated physically and the arc is extinguished completely.

The arc behaviour has been researched widely for a long time [1–7]: interaction between arc and transverse magnetic field or axial magnetic field [1, 2], arc formation [3], computational fluid dynamics analysis for arc flow [4, 5], analysis of arc motion for low-voltage CBs [6, 7] *etc.* According to the research, arc behaviour is largely affected by an insulation medium of CBs. The SF6 gas has a great dielectric property suitable for high-voltage CBs. The vacuum has a good dielectric property, so the vacuum CB (VCB) is popular for medium-voltage levels. The low-voltage CBs generally use the air, which has a low dielectric property due to the expense. In particular, the moulded case CB (MCCB) is a kind of low-voltage CB that employs metal splitter plates to promote the arc extinction. Owing to a recent trend in smart grid power systems, the MCCB requires a remote-controllable actuator. The conventional remote-controllable MCCB used a mechanical actuator with motor-operator. However, there are many drawbacks such as high maintenance cost and low reliability due to numerous mechanical components converting rotational motion to linear motion. Therefore, a linear electromagnetic actuator is expected to solve the conventional motor-operator problem.

So far, the permanent-magnet actuator (PMA), Lorentz force actuator (LA), and separated PMA (SPMA) are kinds of linear electromagnetic actuators. The PMA was proposed for VCB in the 1990s. Though PMA has a simple structure with high reliability, its application limits in the medium-voltage CBs. In the 2000s, LA was proposed and applied to gas CB, VCB, and MCCB [8–10]. Moreover, the SPMA was adapted to VCB [11] and Ro *et al.* [11] presented a possibility that SPMA can be used to low-voltage CBs.

In this paper, all of the conventional linear electromagnetic actuators are investigated in detail to determine which model is the most effective for MCCB. At first, the actuators are designed under the same conditions, and then the characteristics of each actuator are compared with each other. On the basis of the results, the SPMA is designed for 225AF MCCB and compared with the motor-operator and LA of conventional MCCB.

This paper is organised as follows: Section 2 discusses the characteristics and appropriate applications of each linear actuator. Sections 3 and 4 describe the design procedure of SPMA for 225AF MCCB and characteristics compared with existing products. Finally, a conclusion is presented.

## 2 Comparison of linear electromagnetic actuators

### 2.1 Working principle of PMA, LA and SPMA

(i) *Geometry:* A CB consists of arc extinction unit and actuator. As shown in Fig. 1*a*, a normal current flows through loads when fixed contacts are connected with movable contacts. If a fault is detected on a load circuit, then the movable contacts are separated from the fixed contacts by an actuator as illustrated in Fig. 1*b*. The contact spring located between the plunger and movable contacts enables current to flow through loads stably even under the worn contacts.

Figs. 2*a–c* describe the two-dimensional configurations of PMA, LA, and SPMA [7, 8, 11, 12]. In Fig. 2, the magnetic materials establish a path for magnetic field, which is provided by PMs and coils.

(ii) *Working principle:* In case of the PMA, the plunger can remain on top (open state) or bottom (closed state) by magnetic flux of PMs. If a coil is excited, the plunger moves into the direction reducing the reluctance.

The LA is driven by Lorentz force acting on the current-carrying conductors as

$$\boldsymbol{F}_{\mathrm{L}} = I \cdot (\boldsymbol{l} \times \boldsymbol{B}) \tag{1}$$

where $\boldsymbol{F}_{\mathrm{L}}$ is Lorentz force, $I$ is a coil current, $\boldsymbol{l}$ is effective coil length, and $\boldsymbol{B}$ is external magnetic field generated by the PMs aligned on middle. The PMs on top or bottom hold the plunger to prevent a malfunction from unexpected external force.

Finally, SPMA has a separated array of PMs as illustrated in Fig. 2*c*. In general, the closed state requires a higher holding force

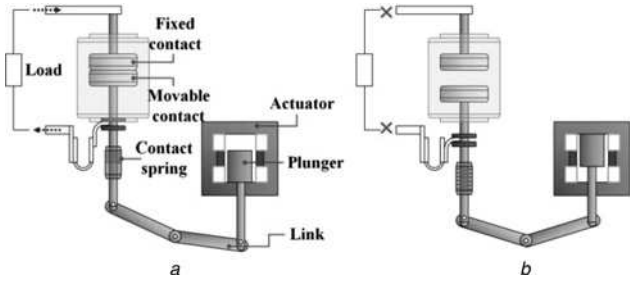


**Fig. 1** *Conceptual schemes of CB during a*

*a* Closed state
*b* Open state

compared with that of the open state due to the repulsive forces of the contact springs. Thus, additional magnets are equipped on bottom to enlarge the closed holding force.

### 2.2 Analysis method

To analyse the current of coil and the operating time, circuit equation of coil and motion equation of plunger should be solved. In circuit equation, the back electro-motive force (EMF) and the linkage flux across the coil are determined by both current of coil and position of plunger. Thus, the circuit equation has to be calculated by coupling with the motion equation to take into account the variation of linkage flux according to the plunger position. To solve the equations, the linkage flux of coil and the electromagnetic force on the plunger in circuit and motion equations are computed from the static finite element method (FEM) analysis. However, the linkage flux and electromagnetic force are varied according to the time due to a non-linearity of magnetic materials. To take account of the variation of the components according to time, the time-differential method (TDM) is applied to the circuit and motion equations [13]. By the TDM, the total calculation time is divided into a small deviation, and then the linkage flux and the electromagnetic force are calculated by the FEM analysis for each step iteratively. The detailed analysis method is presented as follows:

(i) *Static magnetic field analysis by using FEM:* The governing equations for magnetic field analysis can be derived from Maxwell equations, as shown in (2)

$$\nabla \times (\nu \times \boldsymbol{A}) = \mu_0 \mu_r \boldsymbol{J}_0 + \nabla \times (\mu_0 \boldsymbol{M}) \tag{2}$$

where $\boldsymbol{A}$ is the magnetic vector potential, $\mu_0$ is a vacuum permeability, $\mu_r$ is a relative permeability, $J_0$ is the current density for excited coil, and $M$ is the magnetisation for PMs. The linkage flux and electromagnetic force can be obtained by using vector potential distribution, as shown in (3) and (4)

$$\lambda = \sum_{i=1}^{N} \Phi_i = \sum_{i=1}^{N} \left( \oint \boldsymbol{A} \cdot \mathrm{d}\boldsymbol{l} \right)_{i\text{th}} \tag{3}$$

$$F_{\text{mag}} = \iint \left( (\boldsymbol{B} \cdot \boldsymbol{n})\boldsymbol{B}/\mu_0 - \left(B^2 \boldsymbol{n}\right)/(2\mu_0) \right) \mathrm{d}\boldsymbol{s} \tag{4}$$

where $\lambda$ is the total linkage flux of a coil, $\Phi_i$ is the linkage flux in the $i$th turn of a coil, $N$ is the number of turns of a coil, $F_{\text{mag}}$ is the electromagnetic force applied to a plunger, $\boldsymbol{B}$ is the magnetic flux density, $\boldsymbol{s}$ is the surface for calculation region, and $\boldsymbol{n}$ is the normal vector to the surface.

(ii) *Circuit equations and motion equations:* Fig. 2 illustrates the equivalent control circuits for each actuator.

The capacitor voltage, $V_c$, supplies electric power to coils if switch, $S$, is activated. In Fig. 2, $R$ and $L$ are the resistance and inductance of a coil, where the subscripts $c$ and $o$ indicate closing coil and opening coil, respectively. The LA conducts both the closing and opening motion by reversing the current direction in a moving coil, as shown in Fig. 2*b*. Switches $S_3$ and $S_4$ activate the closing, whereas $S_5$ and $S_6$ activate the opening. The circuit

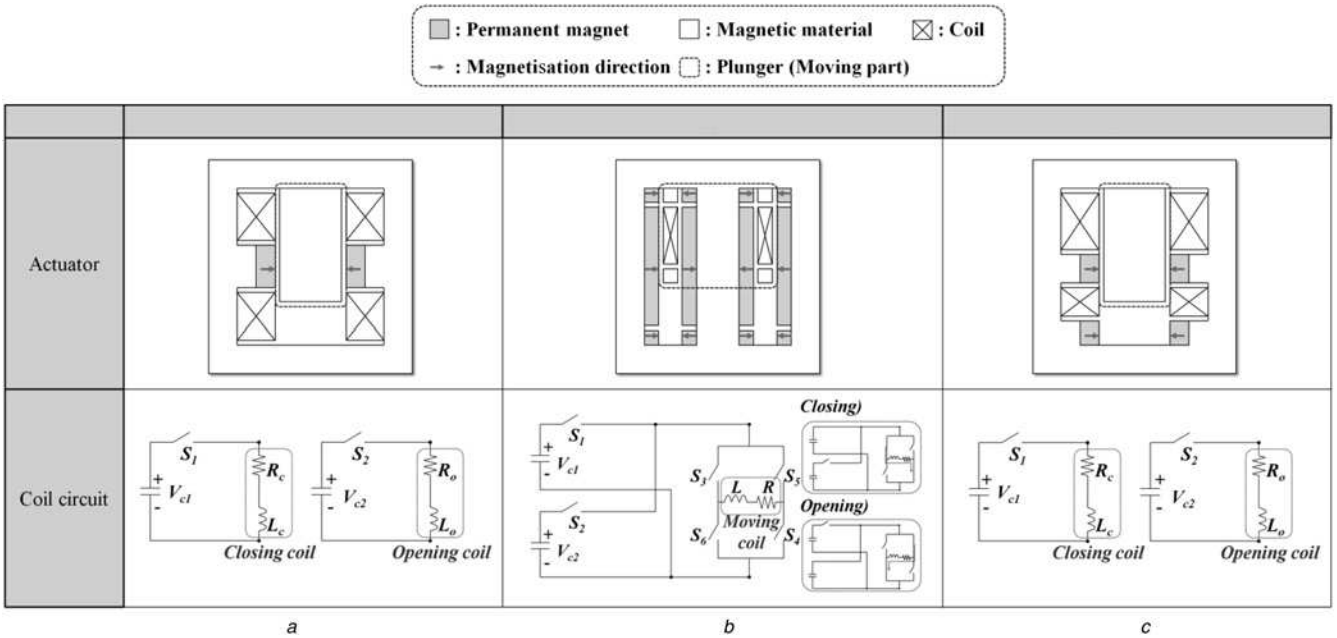


**Fig. 2** *Configurations and equivalent coil circuits for*

*a* PMA
*b* LA
*c* SPMA


*IET Electr. Power Appl.*, 2016, Vol. 10, Iss. 9, pp. 849–857

equation for coil can be expressed by

$$V_c = iR + d\lambda(i, x)/dt \tag{5}$$

where $V_c$ is a capacitor voltage, $i$ is a current, and $x$ is a displacement of the plunger. To predict the back EMF of a coil accurately, the plunger position has to be calculated by (6)

$$m(d^2\boldsymbol{x}/dt^2) = \boldsymbol{F}_{mag} + \boldsymbol{F}_{spring} + m\boldsymbol{g} + \boldsymbol{F}_{fric} \tag{6}$$

where $m$ is the mass of a moving part, $\boldsymbol{F}_{spring}$ is contact springs force acting on the plunger, $m\boldsymbol{g}$ is the gravitational force of a moving part, and $\boldsymbol{F}_{fric}$ is the frictional force.

(iii) *Circuit equations and motion equations coupled with TDM:* The circuit and motion equations with TDM are provided in (7) and (8). The capacitor voltage, $V_C$, can be expressed by excluding a voltage drop from the initial capacitor voltage, as shown in (9)

$$V_c^n = (i^{n-1} + di^n)R + (\lambda^n - \lambda^{n-1})/dt \tag{7}$$

$$m(d^2\boldsymbol{x}^n/dt^2) = \boldsymbol{F}_{mag}^n + \boldsymbol{F}_{spring}^n + \boldsymbol{F}_g^n + \boldsymbol{F}_{fric}^n \tag{8}$$

$$V_c^n = V_c^{n-1} - (i^{n-1} + di^n)\,dt/C \tag{9}$$

where $C$ is a capacitance, $dt$ is the differential time for one step, and the superscript $n$ indicates the $n$th time step. In (7)–(9), the differential current and displacement for the $n$th step, $di^n$ and $dx^n$, can be calculated from the previous-step information. Finally, a current, velocity, and displacement of a plunger for the $n$th step are derived as (10)–(12), respectively

$$i^n = (V_c^{n-1} - (\lambda^n - \lambda^{n-1})/dt)/(R + dt/C) \tag{10}$$

$$\boldsymbol{v}^n = \boldsymbol{v}^{n-1} + (\boldsymbol{F}_{mag}^n + \boldsymbol{F}_{spring}^n + \boldsymbol{F}_g^n + \boldsymbol{F}_{fric}^n)\,dt/m \tag{11}$$

$$x^n = x^{n-1} + \boldsymbol{v}^{n-1}\,dt + 0.5(\boldsymbol{F}_{mag}^n + \boldsymbol{F}_{spring}^n + \boldsymbol{F}_g^n + \boldsymbol{F}_{fric}^n)\,dt^2/m \tag{12}$$

(iv) *Validation of analysis method:* The analysis method of (i)–(iii) used in this research is validated by previous reports [8–11, 14] via applications into various voltage levels and stroke. The stroke indicates a displacement of plunger in actuators during the closing or opening operation. In general, a high-voltage CB requires a long stroke for fast dielectric recovery while a low-voltage CB needs a relatively short stroke. Thus, the high-voltage CB requires high driving force of actuator due to the long stroke. For high-voltage CB, the LA was designed and analysed for 170 kV VCB and 72.5 kV geographical information system by using the analysis method of (i)–(iii) [8, 9]. Furthermore, there are cases of the PMA in 27.5 kV VCB [14], SPMA in 17.5 kV VCB [11], and LA in 225AF MCCB [10] for medium- and low-voltage CB. The correctness of the analysis method used in this research is verified over wide voltage level applications regardless of the stroke from the previous reports.

**Table 1** Requirement for 17.5 kV, 40 kA VCB

| Parameters | Closing | Opening |
|---|---|---|
| capacitor voltage | 100 V | 100 V |
| capacitance | 0.1 F | 0.1 F |
| voltage drop | – | 10 V |
| number of phases | 3 | |
| contact mass | 10.9 kg | |
| guide mass (link, shaft) | 1.7 kg | |
| spring constant | 640,000 N/m/phase | 516,000 N/m/phase |
| vacuum constant | 8333.3 N/m/phase | – |
| holding force | 7100 N | 2000 N |
| actuator stroke | 30 mm | |
| VI displacement | 16 mm | |
| velocity | 0.8–1.2 m/s | 1.2–2.0 m/s |
| operating time | 60 ms | 50 ms |
| actuator depth | 140 mm | |

### 2.3 Design results

In this section, all actuators are optimised to minimise their volumes under 17.5 kV, 40 kA VCB conditions. On the basis of the design results, the most suitable applications for each actuator are proposed:

(i) *Requirements:* The requirements for 17.5 kV, 40 kA VCB are summarised in Table 1 [11].

- *Source:* A capacitor of 100 V, 0.1 F is used as electrical source. The capacitor source should satisfy the operating duty in a sequence of opening–0.3 s rest–closing–opening–15 s rest–closing–opening for 17.5 kV, 40 kA VCB [11]. Thus, the drop of capacitor voltage is restricted to 10 V during the opening in order to fulfil the operating duty.
- *External force acting on the plunger*
  - *Gravitational force of the moving part:* The three contacts and guide weight 10.9 and 1.7 kg, respectively. The guide includes the link, shaft, and anything to support the plunger.
  - *Contact spring force:* The closing is impeded by a repulsive force of contact springs, which is related to a spring constant and a compressed length. The repulsive force of contact springs assists the opening by pushing the plunger at the beginning of the motion.
  - *Vacuum suction force:* In the vacuum interrupter (VI) where contacts exist, a suction force occurs due to the lower internal pressure than external pressure. Hence, the plunger tends to narrow the space between movable contacts and fixed contacts. The vacuum suction force is proportional to a vacuum constant and gap between contacts.

- *Holding force:* The closed holding force has to be higher than 7100 N to hold the plunger against the returning force generated by contact springs. The open holding force requires 2000 N in order to overcome the gravitational force of the plunger and vacuum suction force.
- *Displacement:* The total displacement of the actuator and VI are 30 and 16 mm, respectively. The actuator can operate with a smaller force according to the leverage effect since the actuator displacement is longer than the VI displacement.
- *Velocity of plunger:* The average plunger velocity is measured between 0 and 4 mm of the contact gap. The opening velocity is restricted to 1.2–2.0 m/s for rapid dielectric recovery, whereas the closing velocity is limited to 0.8–1.2 m/s to avoid contacts damage.
- *Operating time:* In a 60 Hz distribution system, a CB has to disconnect a fault current within three cycles of the current (i.e. 50 ms). For the closing, the CB should connect the separated circuits within 60 ms.
- *Actuator depth:* Since the electromagnetic force increases proportionally to the depth of actuator, it is effective to fix the depth on a maximum size. Thus, the depth of all actuators is fixed on 140 mm, which is the allowable size in actuator.

(ii) *Design results:* For the low-voltage CB, the size and cost are the most important factors among characteristics. Thus, the operation time $T$, the current peak $I_p$, and the height of the coil slot $h_s$ are normalised and combined into one objective function $f$ as shown in (13) weighting each parameter as 10, 10, and 80%, respectively

$$f = 0.1 \times \frac{T}{T_{req}} + 0.1 \times \frac{I_p}{I_{req}} + 0.8 \times \frac{h_s}{h_{s,\,max}} \tag{13}$$

The terms $T_{req}$, $I_{req}$, and $h_{s,max}$ stand for the requirements of operation time, current peak, and the allowable space for the coil slot in the actuator. The design variables for each actuator are presented in Fig. 3*a*. The actuators are optimally designed based on the evolution algorithm and the optimised configurations are described

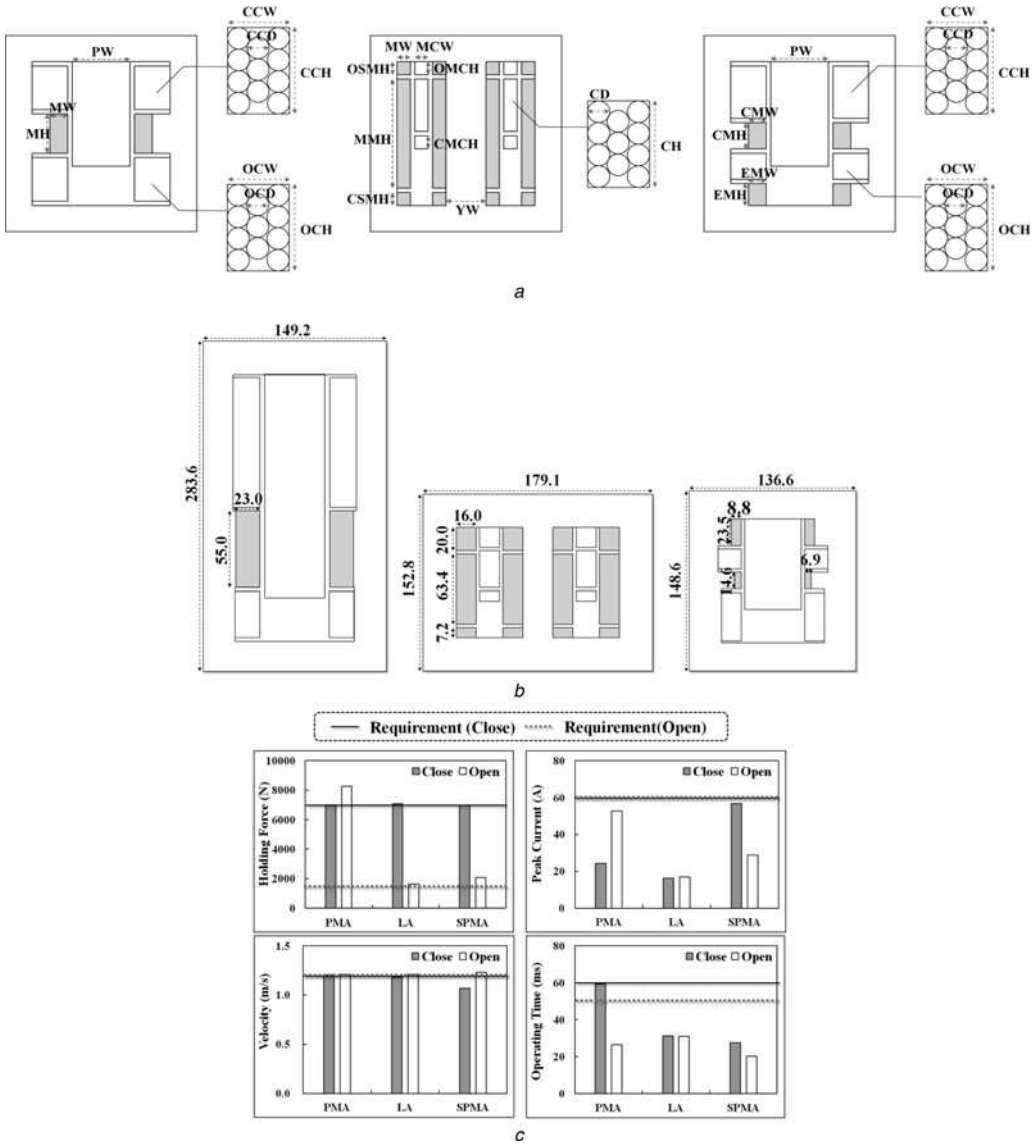


**Fig. 3** *Design variables and design results of each actuator*

*a* Design variables for PMA, LA, and SPMA
*b* Configuration for PMA, LA, and SPMA
*c* Comparison of holding force, peak current, velocity of plunger, and operating time for each actuator

in Fig. 3*b* and Table 2. The PMA occupies the largest volume among the actuators, whereas the LA has the biggest volume of PMs. The actuator cost is associated with the actuator size and PM volume. Thus, the SPMA is superior to the PMA and LA in terms of the size and the cost.

(iii) *Analysis results:* The analysis results of the actuators are presented in Fig. 3*c*.

- *PMA:* PMA has a high open holding force similar to the closed holding force, because it shares common PMs in both the closed and open states. Therefore, a closing coil has to generate high magneto-motive force (MMF). In addition, a large closing coil inductance is required in order to limit the closing velocity under 1.2 m/s. High MMF and closing coil inductance can be achieved simultaneously by increasing the number of coil turns. However, it results in a large closing coil as shown in Fig. 3*b*.
- *LA:* In Fig. 3*c*, the LA generates a high driving force with a smaller current compared with other actuators due to the PM flux contributing to Lorentz force. However, it is impossible to obtain the best closing and opening performance. Moreover, many PMs with complex moving parts increase the manufacturing cost of LA.
- *SPMA:* Owing to the separated PMs, the holding force for the closed and open states can be independent of each other. Therefore, the SPMA can have a reduced closing coil size and an improved closing performance compared with the PMA. Furthermore, the opening and closing characteristics can be separated by using distinct coils during the closing and opening.

**Table 2** Total volume and magnet usage for optimised three actuators

| | PMA | LA | SPMA |
|---|---|---|---|
| total volume, $cm^3$ | 5.92 | 3.83 [a] **(35.3%↓)** | 2.84 [a] **(52.0%↓)** |
| magnet usage, $cm^3$ | 0.35 | 0.81 [a] **(131.4%↑)** | 0.09 [a] **(74.3%↓)** |

[a]The values of percentage indicate relative characteristics as compared with those of the PMA. It can help evaluating the relative manufacturing cost and compactness for each actuator

## 2.4 Discussion

The characteristics are tabulated in Table 3. The SPMA can be applicable to low-voltage CBs, whereas the PMA and LA are


*IET Electr. Power Appl.*, 2016, Vol. 10, Iss. 9, pp. 849–857

**Table 3** Comparison of characteristics for three actuators

| | | PMA | LA | SPMA |
|---|---|---|---|---|
| characteristics | cost[a] | low | high | low |
| | size[a] | large | medium | small |
| | driving force[b] | low | high | medium |
| reliability and life-cycle | | high | medium | high |
| suitable applications | | medium voltage | high voltage | low–medium voltage |

[a]Dominant characteristics for a low-voltage and medium-voltage applications
[b]Dominant characteristics for a high-voltage application

difficult to commercialise for low-voltage applications due to the cost and size. In addition, the SPMA has a high reliability, and long life-cycle analogous to the PMA because of a simple structure. However, the LA is organised with lots of components in the plunger and control circuit. The plunger comprised of the moving coil and magnetic materials require manual fabrication. It can lower a fabrication tolerance and cause a decrease of reliability. Furthermore, frequent failures occur in switching devices on the control circuit. Therefore, the LA has a relatively low reliability and life-cycle compared with the PMA and SPMA. Consequently, the SPMA is the most effective actuator for a low-voltage CB, MCCB.

## 3 Design and analysis of SPMA for 225AF MCCB

### 3.1 Geometry and working principle of MCCB

Fig. 4 presents the MCCB driven by SPMA and the equivalent control circuits.

The actuator provides a mechanical energy for the movable contacts via a rotational disk. During the closing, where switch $S_1$ is on and $S_2$ is off, the rectified AC power supplies electric power to a closing coil and charges the capacitor. During the opening, where switch $S_1$ is off and $S_2$ is on, the electric power of the capacitor is discharged through an opening coil.

### 3.2 Optimal design

(i) *Requirements:* The requirements for 225AF MCCB are presented in Table 4 [10]. The MCCB has to break four phases including three phase lines and one neutral line, within one cycle

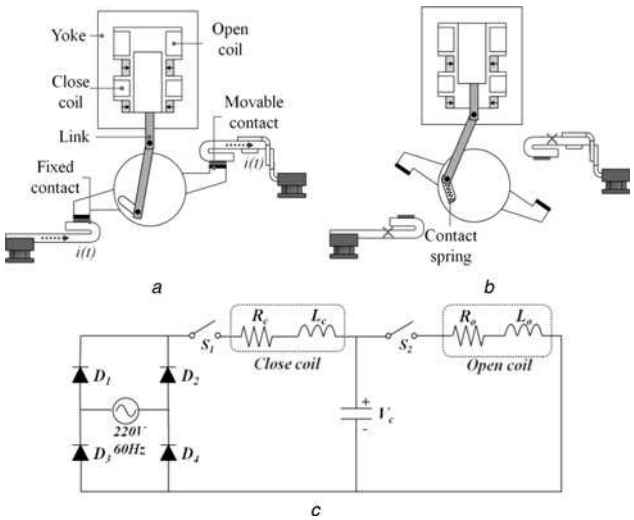


**Fig. 4** *Structure of the MCCB driven by SPMA*

*a* Closed state
*b* Open state
*c* Equivalent control circuit

**Table 4** Requirements for 225AF MCCB

| Source | Closing Rectified 220 V/60 Hz | Opening Capacitor 250 V/100 μF |
|---|---|---|
| peak of current | 10 A | |
| number of poles | 4 | |
| contact mass | 0.02 kg/pole | |
| guide mass | 0.02 kg | |
| spring force | 2.3 kg/pole | |
| holding force | 150 N | 110 N |
| actuator stroke | 5.4 mm | |
| VI displacement | 9.6 mm | |
| operating time | – | 17 ms |
| actuator depth | 50 mm | |

of the current (i.e. 17 ms). The actuator depth is determined based on available actuator space.

(ii) *Proposed multi-step optimisation strategy:* For the SPMA, the size of magnets, yoke, and coil specification have an effect on the actuator performances. However, it is difficult and time-consuming to take account of those design variables all together. Therefore, this paper proposes a multi-step optimisation strategy to mitigate computational burden of optimisation. The proposed optimisation strategy proceeds in a sequence of *holding force on the close and open states, closing performance,* and *opening performance* as shown in Fig. 5. The individual optimisation stage has different design variables and objective functions. Furthermore, their design variables are independent with each other's objective function. At each stage, best solutions can be found from a surrogate model, which is obtained by limited number of sampled data. In this paper, the surrogate model is estimated simply by using cubic spline method since a non-linear property does not appear significantly on actuator performance. The optimisation method is explained step by step as follows.

*3.2.1 Definition of design variables and upper and lower bounds:* Figs. 5*b* and *d* illustrate the design variable at each optimisation stage.

*Design variables for holding force on the close and open states*

- *End magnet height (EMH) and central magnet height (CMH):* The augmentation of magnet volume increases the holding force directly. Except the magnet width, the height of magnets defined by EMH, CMH are considered as design variables because a variation of magnet width has relatively low influences on the holding force. When the magnet width increases, the operating point of magnets gets lower due to the enlarged reluctance of magnet. Thus, the magnet width is not an effective factor for the holding force because of the trade-off relation between the operating point and the MMF. In contrast, the increase of the magnet height leads to the significant improvement of both the operating point and the MMF of magnets. Therefore, a long-shaped magnet is preferred to a wide one under the same volume. Since the MCCB focuses on the compactness and the manufacturing cost, the EMH and the CMH are designed fixing the width of magnets as 2 mm, which is a minimum length to prevent the irreversible degradation and the mechanical damage of magnets. The bounds of EMH and CMH are 2–5 mm as shown in Tables 5 and 6 taking into account the manufacturing and the available space of actuator.
- *Plunger width (PW):* The holding force depends on the product of the air-gap magnetic flux density and the plunger surface, which can be controlled by the PW. In this paper, the bounds of PW are 4–15 mm taking account the durability and the available space of actuator. The width of yoke is fixed on a half of the PW so that the flux density of the yoke to be equal to that of the plunger.

*Design variables for closing performances*

- *The number of turns of closing coil in x ($N_{cx}$) and y ($N_{cy}$):* The number of turns $N_{cx}$ and $N_{cy}$ determines both the resistance and

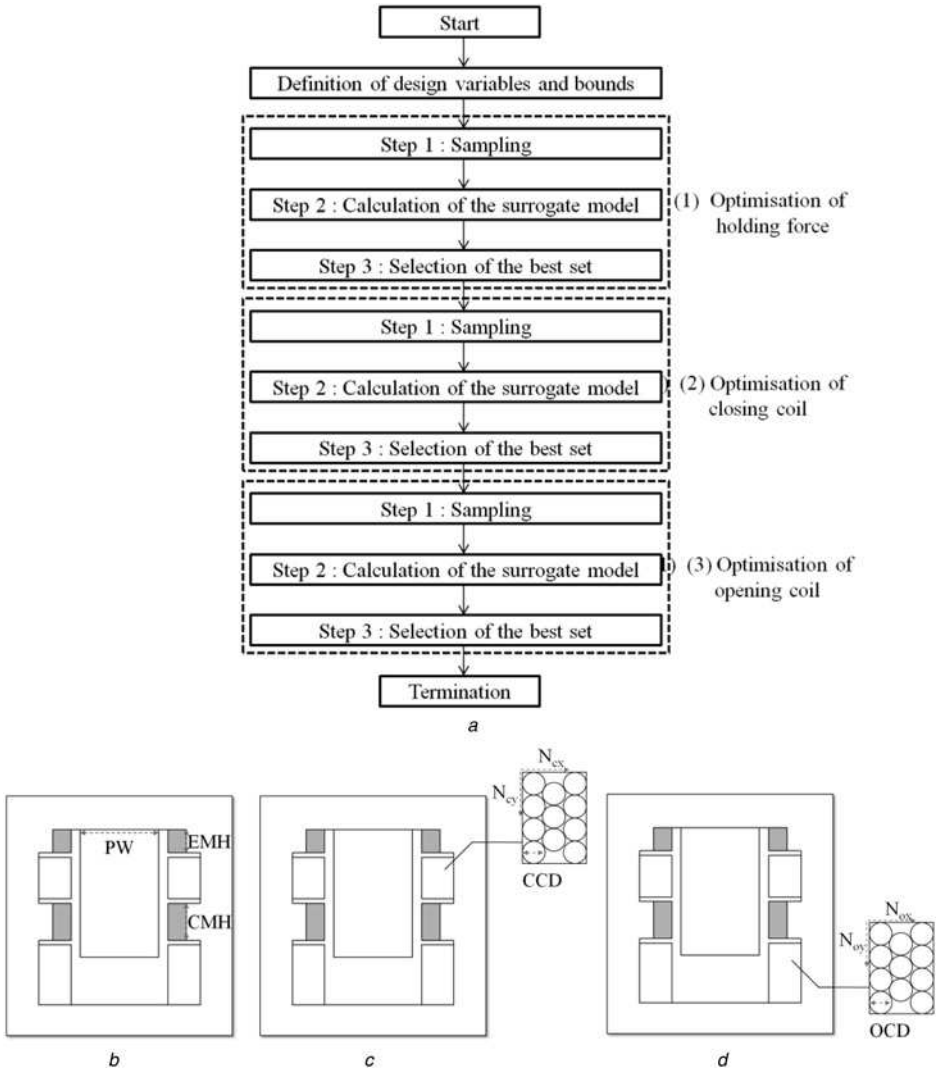


**Fig. 5** *Optimisation method and design variables*

*a* Flowchart of the multi-step optimisation strategy
*b* Design variables for close/open holding force
*c* Design variables for closing performance
*d* Design variables for opening performance

the inductance. The MMF of closing coil, which is a dominant factor for closing performance, can be defined by a product of the resultant current and the total number of turns. In Table 5, the bounds of $N_{cx}$ and $N_{cy}$ are 21–25 and 17–23, respectively, based on the available space of actuator and the least MMF required for the closing.

- *Closing coil diameter (CCD):* The CCD is one of the main parameters for the resistance and the inductance. In Table 5, the bounds of CCD are determined as 0.19–0.23 mm taking into account the size of actuator and the required MMF for closing.

*Design variables for opening performances*

- *The number of turns of opening coil in x ($N_{ox}$) and y ($N_{oy}$), and opening coil diameter (OCD):* Similar to the closing case, the $N_{ox}$, $N_{oy}$, and OCD are selected for design variables in order to control the MMF of opening coil. The opening coil should produce large electromagnetic force enough to overcome the close holding force, which is higher than the one with open state. Since the opening needs higher MMF than the closing, the bounds of opening coil are selected for closing as displayed in Table 5.

**Table 5** Variation width and the number of initial sampling of design variables

| Design variables | Variation width | The number of initial sampling |
|---|---|---|
| EMH | 2–5 mm | 4 |
| CMH | 2–5 mm | 4 |
| PW | 4–15 mm | 4 |
| $N_{cx}$ | 21–25 | 3 |
| $N_{cy}$ | 17–23 | 4 |
| CCD | 0.19–0.23 mm | 3 |
| $N_{ox}$ | 24–28 | 3 |
| $N_{oy}$ | 24–30 | 4 |
| OCD | 0.22–0.26 mm | 3 |

### 3.2.2 Optimisation of holding force:

*Step 1: Sampling:* For the design of close and open holding force, EMH, CMH, and PW are

**Table 6** Performance of MCCB driven by the motor-operator, the LA, and the SPMA

| | Motor-operator | LA | | SPMA | |
|---|---|---|---|---|---|
| | | Actuator | Drive | Actuator | Drive |
| volume, $cm^3$ | 0.90 | 0.15 | 0.21 | 0.04 | 0.03 |
| operating time, ms | 310/230 (closing–opening) | <10 | | <10 | |
| power, W | 14 | 500/760 (closing–opening) | | 600/150 (closing–opening) | |


*IET Electr. Power Appl.*, 2016, Vol. 10, Iss. 9, pp. 849–857

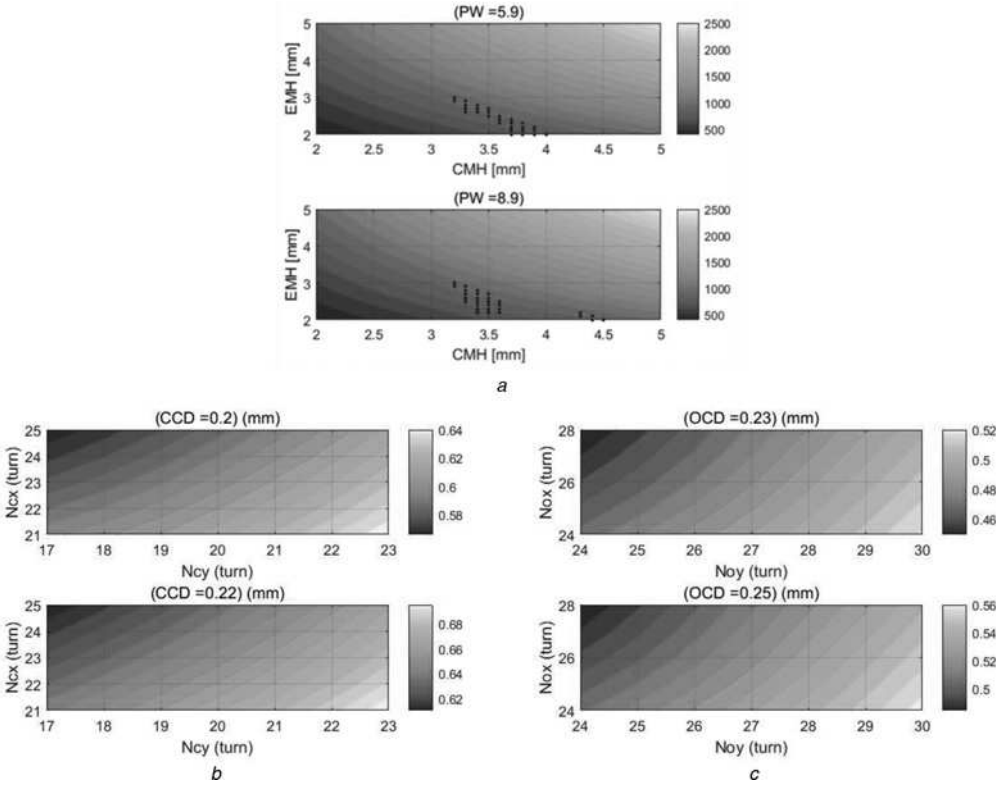


**Fig. 6** *Surrogate model of objective function for*

*a* Close and open holding force $g_1$
*b* Closing characteristics $g_2$
*c* Opening characteristics $g_3$

sampled at $4 \times 4 \times 4$ data points as shown in Table 5. The objective function for holding force optimisation $g_1$, close holding force $f_C$, and open holding force $f_O$ are evaluated at sampled 64 points. In this paper, the objective function $g_1$ is defined by

$$g_1 = V_m \tag{14}$$

In (14), $g_1$ is organised with the magnet volume $V_m$, which is one of the most important factors for a manufacturing cost of the MCCB.
*Step 2: Calculation of the surrogate model:* The surrogate model of objective function $g_1$, close holding force $f_C$, and open holding force $f_O$ can be estimated by interpolating the sampled data. The cubic spline is employed as an interpolation method in this research.
*Step 3: Selection of the best set:* The objective values, close holding force $f_C$, and open holding force $f_O$ are estimated at each feasible point by using surrogate models. Finally, the best solution, which has a minimum volume of magnets to satisfy boundary condition (15), is selected

$$145.5\,\text{N} \le f_C \le 165\,\text{N}, \quad 106.7\,\text{N} \le f_O \le 121\,\text{N} \tag{15}$$

In other words, the close and open holding force is restricted between 97 and 110% of the requirements 150 and 110 N. The holding force close to the requirements is preferable because the excessive holding force over the requirements impedes an initial motion during the closing and opening. Moreover, high MMF is necessary enough to overcome the large holding force and it induces the problems such as the augmentation of volume for coil slots and the increase of current peak. Therefore, the close and open holding force is restricted below 110% of the requirements as indicated in (15).

*3.2.3 Optimisation of closing coil:* *Step 1: Sampling:* For a closing coil design, $N_{cx}$, $N_{cy}$, and CCD are sampled at $3 \times 4 \times 3$ points as shown in Table 5. In the closing optimisation, the operating time $T_c$, the current peak of closing coil $I_{cp}$, and the height of closing coil slot $h_{cc}$ are significant performances to be considered. In this paper, each component is normalised and combined into one objective function $g_2$

$$g_2 = w_1 \frac{T_c}{0.017} + w_2 \frac{I_{cp}}{10} + w_3 \frac{h_{cc}}{h_{cc,\,max}} \tag{16}$$

where $w_1$, $w_2$, $w_3$, and $h_{cc,max}$ stand for the weights for each term, and maximum $h_{cc}$ in the calculation domain. To balance the influences of characteristics on the objective function, each term of (16) is normalised by 0.017 s, 10 A, and $h_{cc,max}$ which presents the maximum values within the calculation region. The weights $w_1$, $w_2$, and $w_3$ are selected depending on the importance of each term. In this paper, the weights $w_1$, $w_2$, and $w_3$ are determined empirically as 15, 40, and 45% since the power consumption and the size of actuator are more important factors than the operating time for the low-voltage level CB as the MCCB. The power consumption and actuator size depend on the current peak $I_{cp}$, and the height of closing coil slot $h_{cc}$.
*Step 2: Calculation of the surrogate model*: On the basis of the sampled data, a surrogate model for closing objective function is interpolated by using cubic spline method in this step.
*Step 3: Selecting the best set:* In the surrogate model, the objective values are calculated at points which are selected considering manufacturability. Among the selected points, the point where the objective value is a minimum is selected as the best set.

*3.2.4 Optimisation of opening coil:* *Step 1: Sampling:* For an opening coil design, $N_{ox}$, $N_{oy}$, and OCD are sampled with $3 \times 4 \times 3$ points, respectively. The objective function for opening is induced by

$$g_3 = w_1 \frac{T_o}{0.017} + w_2 \frac{I_{op}}{10} + w_3 \frac{h_{oc}}{h_{oc,\,max}} \tag{17}$$

where $T_o$, $I_{op}$, $h_{oc}$, and $h_{oc,max}$ denote the operating time for opening, the current peak of the opening coil, the height of the opening coil slot, and the maximum $h_{oc}$ in the calculation domain. The weights $w_1$, $w_2$, and $w_3$ are determined as 15, 40, and 45% in the same way with the closing.

*Step 2: Calculation of the surrogate model:* Similarly, a surrogate model for opening objective function can be gained by interpolating the sample data.

*Step 3: Selection of the best set:* The objective values for each feasible point can be computed by a surrogate model and the best solution minimising the objective function is selected in this step.

(iii) *Optimisation results:* The optimisation is terminated if best solutions are found for all of design steps. The detailed optimisation results for MCCB are as follows.

*3.2.5 Optimisation of holding force:* The holding force increases when EMH and CMH are enlarged. If the PW decreases, increase of the air-gap flux density raises the holding force until the saturation appears significantly in the core. When the core is saturated heavily, the air-gap flux density cannot be raised anymore and the surface of plunger continuously decreases, thereby dropping the holding force.

A surrogate model for close and open holding force is related to the magnet volume, which is determined by CMH and EMH as illustrated in Fig. 6*a*. The black dots in Fig. 6*a* describe candidate solutions satisfying the close and open holding force conditions of (15). They are distributed non-linearly because of the saturation effects.

The average differences between the holding forces calculated by the interpolation and the FEM are estimated to 0.96 and 0.51%, respectively, at the close and open states. Accordingly, the interpolation results show a good agreement with the FEM analysis results. The best set for PW, CMH, and EMH is chosen as 8, 4.1, and 2.3 mm, respectively. In this case, the close holding force and open holding force are evaluated to 165 and 107 N, respectively.

*3.2.6 Optimisation of closing coil:* A current peak of closing coil is mitigated if the number of coil turns and coil resistance are increased. The operating time depends on MMF defined as the product of the turns and the current of the coil. When the number of turns of coil increases, the current peak gets lower. Thus, the total MMF and operating time has a non-linear property according to the variations of $N_{cx}$ and $N_{cy}$. In contrast, the large CCD results in low resistance and high current, thereby improving the operating time.

Fig. 6*b* presents the surrogate model for objective function for closing (16). The best set for $N_{cx}$, $N_{cy}$, and CCD is selected as 21, 18, and 0.19 mm, respectively. The average difference for operating time and current peak between interpolation results and FEM analysis results is evaluated as 0.30 and 0.07%, respectively. Furthermore, the calculation time can be saved by 80% compared with the calculation time for the characteristic analysis by using the FEM about all data points.

*3.2.7 Optimisation of opening coil:* A variation of opening characteristics according to the design variables shows a same tendency with that of the closing. Fig. 6*c* depicts the surrogate model of opening objective function (17) and the best solution for $N_{ox}$, $N_{oy}$, and OCD is selected as 24, 26, and 0.22 mm. The average differences for the operating time and the current peak between the interpolation result and the FEM analysis result are evaluated as 0.59 and 0.11%, respectively.

*3.2.8 Experiments:* The prototype is manufactured based on the design results and employed in 225AF MCCB [15] as shown in Fig. 7*a*. The commercial electric power is supplied to a control circuit as explained in Section 3.1. The current of the closing and opening coil shows a transient response since the reluctance and the inductance show a large variation according to the variation of position of plunger. Therefore, the characteristics of SPMA can be verified through a current waveform because the current waveform reflects the displacement of plunger as well as circuit information. In Figs. 7*b* and *c*, the analysis results agree with the experimental results well during both closing and opening cases. In Figs. 7*b* and

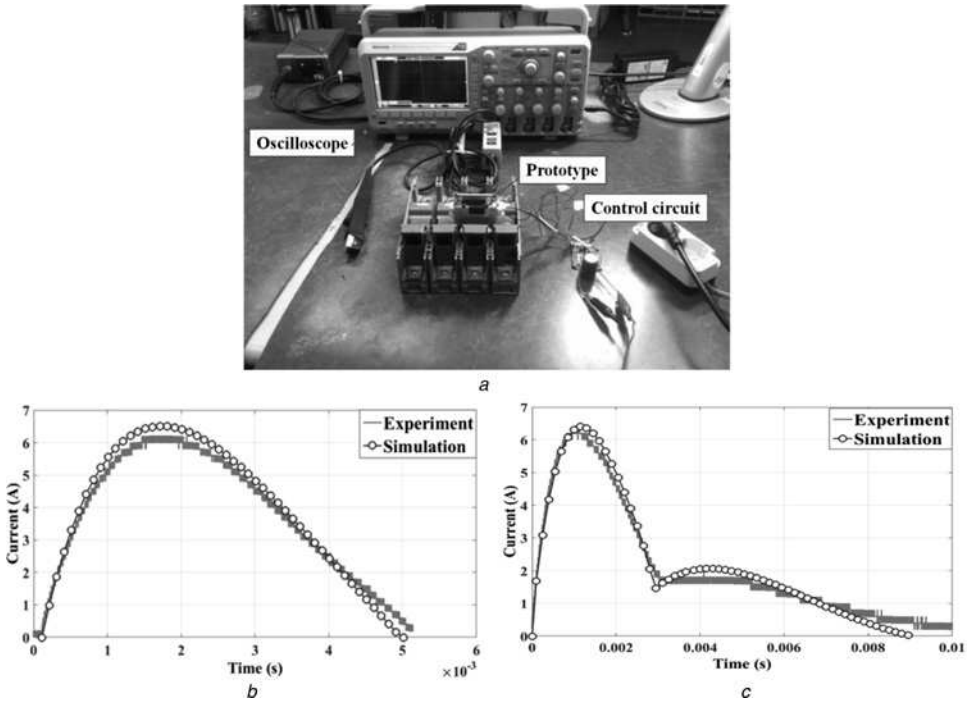


**Fig. 7** *Experimental setup and experimental results*

*a* System of prototype and experimental setup
*b* Current waveform of closing coil
*c* Current waveform of opening coil


*IET Electr. Power Appl.*, 2016, Vol. 10, Iss. 9, pp. 849–857

*c*, it can be seen that a slight error is caused mainly by the mechanical factors such as the friction force, the spring load *etc.*

*Closing operation:* In the initial operation, a current of the closing coil is increased by the electrical input power source. When the closing coil generates high MMF enough to overcome the holding force, the plunger starts to move, and then a back EMF is induced on the closing coil to interrupt the plunger motion. Especially, the back EMF caused by a variation of plunger location is termed as motional EMF in this paper. Thus, the current of closing coil is declined by the motional EMF as shown in Fig. 7*b* at 1.7 ms. At this point, the error of peak current is estimated to 4.8%. After the capacitor illustrated in Fig. 4*c* is fully charged, the input current of closing coil comes to be a zero.

*Opening operation:* The opening coil is activated by the capacitor, which is charged during the closing operation. The current of opening coil increases during the initial operation, but is decreased by the motional EMF at 1.5 ms. The error of current peak is evaluated to 0.1%. When the opening is completed, the motional EMF decreases to a zero. Hence, the current of opening coil increases temporally after the opening is completed at 3 ms as displayed in Fig. 7*c*. However, the current is declined again as the capacitor dissipates continuously its stored electric energy.

## 4 Comparison between designed MCCB and conventional MCCBs

Table 6 presents the performance of the MCCB driven by the motor-operator, the LA, and the SPMA.

- *Volume:* The motor-operator occupies the biggest volume among the actuators. By reducing mechanical components, the LA volume can be decreased by 60% compared with the motor-operator. However, LA requires the switching device inside a drive. The switching device is broken frequently and occupies a large volume. However, the MCCB driven by SPMA can operate without any switching devices. Therefore, the size of driver is reduced remarkably. Furthermore, the size of actuator is reduced by 75% compared with the LA due to a superior working principle for low-voltage level CBs.
- *Operation time and power consumption:* The SPMA and LA consume much more power than the motor-operator. However, the SPMA and LA use lower energy than the motor-operator since the motor-operator works over a long time. In addition, the SPMA requires lower energy during the opening operation than the LA, because the SPMA has separated coils for the opening and closing and they can be designed optimally to satisfy each requirement corresponding to opening and closing operations. Therefore, the SPMA is the most outstanding actuator in the aspect of the size, the cost, and the energy consumption.

## 5 Conclusions

Owing to the trend of IT and the automation of electric power system, the demand for a remote-controllable electromagnetic actuator for CB has increased dramatically. Therefore, the useful guideline for the selection of the most effective actuator for a diverse voltage level of CB is proposed in this paper.

In this research, it is verified that the SPMA is the most suitable actuator for low-voltage level CB and superior to the conventional actuators in the aspect of performance, cost, and size. Furthermore, in this paper, the multi-step optimisation strategy is proposed for the optimal design of the SPMA and the SPMA is designed optimally for the application of MCCB. Accordingly, this paper can eventually contribute to the smart grid and automation of electric power system.

## 6 Acknowledgments

This work was supported by the Brain Korea 21 Plus Project, KD Power, and Seoul National University Electric Power Research Institute.

## 7 References

1 Delachaux, T., Fritz, O., Gentsch, D., *et al.*: 'Numerical simulation of a moving high-current vacuum arc driven by a transverse magnetic field (TMF)', *IEEE Trans. Plasma Sci.*, 2007, **35**, (4), pp. 905–911
2 Lamara, T., Gentsch, D.: 'Theoretical and experimental investigation of new innovative TMF–AMF contacts for high-current vacuum arc interruption', *IEEE Trans. Plasma Sci.*, 2013, **41**, (8), pp. 2043–2050
3 Cao, Y., Zhao, J., Li, J., *et al.*: 'Dynamic model simulation of arc formation in vacuum circuit breaker'. Int. Symp. Discharges and Electrical Insulation in Vacuum, Braunschweig, 2010, pp. 435–438
4 Park, S.H., Bae, C.Y., Kim, H.K., *et al.*: 'Computer simulation of interaction of arc-gas flow in SF6 puffer circuit breaker considering effects of ablated nozzle vapor', *IEEE Trans. Magn.*, 2006, **42**, (4), pp. 1067–1070
5 Park, J.H., Kim, K.H., Yeo, C.H., *et al.*: 'CFD analysis of arc–flow interaction in a high-voltage gas circuit breaker using an overset method', *IEEE Trans. Plasma Sci.*, 2014, **42**, (1), pp. 175–184
6 Degui, C., Xingwen, L., Liang, J., *et al.*: 'Numerical simulation of arc motion during interruption process of low-voltage circuit breakers'. 26th Int. Conf. Electrical Contacts, Beijing, 2012, pp. 255–260
7 Liu, Y., Yuan, H., Chen, D., *et al.*: 'Experiment and simulation research on the influence of different main contact system on the interruption performance of control and protective switch', *IEEE Trans. Power Deliv.*, 2010, **25**, (3), pp. 1556–1563
8 Kang, J.H., Choi, S.M., Dong, E.Y., *et al.*: 'Development of electromagnetic actuator for hybrid type gas insulated switchgear'. 2007 Int. Conf. Power Engineering, Energy and Electrical Drives, Setubal, 2007, pp. 499–503
9 Kang, J.H., Kwak, S.Y., Kim, R.E., *et al.*: 'The optimal design and dynamic characteristics analysis of electric actuator (EMFA) for 170 kV/50 kA VCB based on three-ink structure'. 23rd Int. Symp. Discharges and Electrical Insulation in Vacuum, Bucharest, 2008, pp. 177–180
10 Hong, S.K., Bae, B.J., Cho, D.J., *et al.*: 'Design and electromagnetic force driving actuator (EMFA) and linkage for molded case circuit breaker'. 2010 Int. Conf. Electrical Machines and Systems, Incheon, 2010, pp. 1573–1577
11 Ro, J.S., Hong, S.K., Jung, H.K.: 'Characteristic analysis and design of a novel permanent magnetic actuator for a vacuum circuit breaker', *IET Electr. Power Appl.*, 2013, **7**, (2), pp. 87–96
12 Fang, S., Xia, M., Lin, H., *et al.*: 'Analysis and design of a high-speed permanent magnet characteristic actuator using eddy current effect for high-voltage vacuum circuit breaker', *IET Electr. Power Appl.*, 2016, **10**, (4), pp. 268–275
13 Ro, J.S., Park, H.J., Jung, H.K.: 'Characteristic analysis and design of a novel Lorentz force driving actuator for a molded case circuit breaker', *IET Electr. Power Appl.*, 2015, **9**, (1), pp. 1–9
14 Li, W., Fang, C.E., Zhou, L., *et al.*: 'Simulation and testing of operating characteristic of 27.5 kV vacuum circuit breaker with permanent magnetic actuator'. 23rd Int. Symp. Discharges and Electrical Insulation in Vacuum, Bucharest, 2008, pp. 125–128
15 Park, H.J., Kim, S.H., Ro, J.S., *et al.*: 'Design and analysis of molded case circuit breaker for 225AF'. Korean, the KIEE Spring Conf., 2014